Journal of Materials Chemistry A

Accepted Manuscript

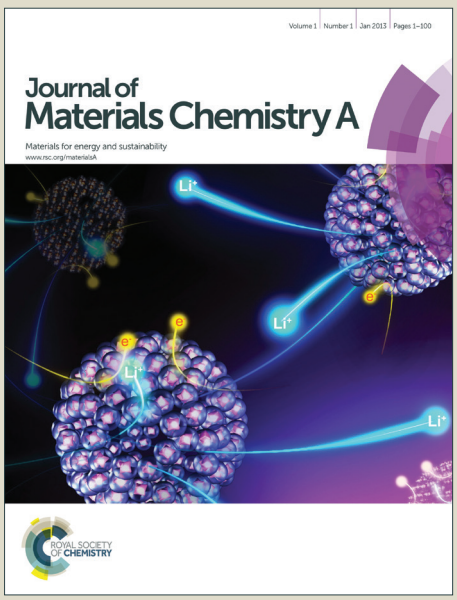

ROYAL SOCIETY OF CHEMISTRY

www.rsc.org/materialsA

Journal of Materials

Chemistry A

RSCPublishing

ARTICLE

Flexible and highly stable electrospun nanofibrous membrane incorporating gold nanocluster as a efficient probe for visual colorimetric detection of Hg(II)

Cite this: DOI: 10.1039/x0xx00000x

Received 00th May 2014,
Accepted 00th May 2014

DOI: 10.1039/x0xx00000x

www.rsc.org/

Anitha Senthamizhan,*[,a] Asli Celebioglu,[a,b] Tamer Uyar[a],[b,*]

Here, we have conferred the visual colorimetric detection of Hg^{2+} based on flexible fluorescent electrospun nanofibrous membrane (NFM). It is an efficient approach, in which we have effectively integrated the fluorescent gold nanoclusters (AuNC) into electrospun polyvinyl alcohol (PVA) nanofibers. Interestingly, the consequential composite nanofibers (AuNC*NFM) have shown to retain their fluorescence properties of AuNC and have exhibited a ray of red fluorescence under UV light, completing a cogent criteria for the production of a visual colorimetric sensor. Furthermore, capabilities with regard to the stability of AuNC*NFM has been under observation for a period of six months, with fitting conditions of typical atmosphere and the resulting outcome has thrown light on their long term storability and usability. It is clear from the fact that the nanofibrous membrane characteristic to preserve their fluorescence ability up to a temperature of 100 ºC does not have an effect on the sensing performance in the real time application. The water insoluble AuNC*NFM have been successfully tailored by crosslinking with glutaraldehyde vapor. Further, the contact mode approach has been taken into consideration for the visual fluorescent response Hg^{2+} and the observed change of color recognizes their utility for an onsite detection of Hg^{2+} with a detection limit of 1 ppb. The selectivity of the AuNC*NFM hybrid system has been analysed by its response to other common toxic metal interferences (Pb^{2+}, Mn^{2+},Cu^{2+}, Ni^{2+}, Zn^{2+}, Cd^{2+}) in water. Several unique features have been surveyed of the hybrid system including high stability, self standing, naked eye detection, selectivity, reproducibility and easy handling, setting a new trend in the membrane based sensor system.

Introduction

Water serves as a essential and vital need for the wellbeing and sustenance of life. In some cases, however, the water quality gets a chance to be compromised by the presence of infectious agents and toxic metals.[1] This effect primarily caused by industry, agricultural and household means eventually causes damage to the environment and human health. Among these many causes of water pollution, those generated by the use of heavy metal ions poses a serious threat to mankind and has been a topic of concern for decades now. Most importantly, mercury stands out as a fine example of heavy metal ions causing damage to the nervous system even when present in parts per million concentration (ppm). Using extensive research and exploration, it has been comprehensive that the level of mercury to its maximum level in drinking water amount to just about 2 parts per billion (ppb), as per the norms defined by the United States Environmental Protection Agency (US-EPA).[2]

The Hg^{2+} has commemorated various environmental and health problems evoking high interest and speculation to further down research for identifying and eradicating the toxic components in water. Over the past few decades, various techniques have been devised for monitoring the mercury levels using atomic absorption spectroscopy, electrochemical sensors, chromatography and several other techniques.[3-9] But, most of them bear certain disadvantages of multistep sample preparation and also prove to be expensive. Amongst all these techniques, colorimetric assay of Hg2+ has gained a lot of attention among scientists owing to its convenience, facile monitoring, and no requirement of sophisticated instruments. [10-12] The application of noble metal nanoparticles for the water

purification and their contribution to detect the toxic metals dates back to a long time. Besides, recent effort on fluorescent gold nanoclusters has made it a new platform for developing mercury sensors owing to their promising characteristics of operational simplicity, cost-effectiveness, easy visualization and high sensitivity.[13-18] However, the reported techniques, being mostly solution-based have resulted in stability problems, limiting their potential ability and practical applications. Moreover, a sensing mediator is used to be mixed with the analyte medium and the corresponding responses are monitored in situ, with respect to optical responses making the sensor inefficient. This necessitates a need to develop a novel and modernistic method to fabricate a solid template-based sensor on a large scale for technological applications.[19-22]

To make this possible for usage in day to day life, luminescent metal clusters are designed and integrated into the solid matrix which provide an easy platform to maintain their stability and easy accessibility for probe analytes. However, due to the solid support having a low specific surface area, it affects the reactivity and sensitivity of the sensor performance.[23-30] The features of a high surface area and good flexibility are supposed to replenish these detriments. When comparing all the other techniques, electrospinning provides versatility for the fabrication of functional nanofibers and incorporation of active agents into the nanofiber matrix.[31-32] Essentially, electrospun nanofibrous membranes are flexible, cost effective, relatively easy to handle and have accurate reproducibility.

Herein, we present an effectual synthesis procedure to produce highly luminescent gold nanoclusters (AuNC) embedded in electrospun polyvinyl alcohol (PVA) nanofibrous membrane (NFM) termed as AuNC*NFM for efficient detection of Hg^{2+}. However, fabricating flexible polymeric nanofibrous membrane composed of AuNC for sensing applications raises several issues that need to be addressed, regarding the aggregation, fluorescence quenching in the nanofibers, and their stability over time and temperature. In order to find a paramount solution to these requirements, a suitable polymer matrix that does not quench the luminescence intensity of AuNC is to be chosen. Another vital concern to be considered is the incorporation of the aqueous AuNC into a hydrophobic polymer matrix due to their incompatibility. Consequently, PVA is chosen as a support matrix due to their non toxicity, electrospinnablity, and their compatibility. All the same, the obtained nanofibrous composite mat is instantaneously dissolved in water further limiting its applications. Thus, the water-insoluble PVA nanofibrous mat is prepared by cross-linking with glutaraldehyde (GA) vapour for an optimal period of time and suitable concentration.

Experimental Section

Materials and Methods

Tetrachloroauric acid trihydrate ($HAuCl_4 \cdot 3H_2O$, Sigma Aldrich), bovine serum albumin (BSA, Sigma Aldrich), polyvinyl alcohol (PVA, Scientific Polymer, 88% hydrolyzed, Mw 125,000), Mercuric acetate (Merck), Zinc acetate dihydrate (Sigma Aldrich, ≥98%), Lead(II) nitrate (Sigma Aldrich, ≥99.0%) Copper(II) acetate hydrate (Sigma Aldrich, 98%), Cadmium nitrate tetrahydrate (FLUKA) and Cobalt(II) acetate tetrahydrate (SIAL) were purchased. The deionized water was used from the Millipore Milli-Q Ultrapure Water System. Stock solution of metal ions (50 ppm) prepared in de-ionised water and further standard solution used for calibration were prepared by gradually diluting the stock solution in water with concentration range from 50 ppm to 10 ppt.

Preparation of fluorescent gold nanocluster (AuNC)

The fluorescent gold nanocluster was performed according to the previously reported method.33 By the method previously described, approximately 10 mM of HAuCl4 solution (10ml) was added to an equal amount of BSA solution (50 mg mL−1) at 37°C with vigorous stirring. Two minutes later, 1 ml of 1 M NaOH solution was introduced into the mixture, and the reaction was allowed to proceed accompanied by vigorous stirring at 37°C for a time period of 12 hours. The thus prepared AuNC emitted red fluorescence under exposure to UV light, further which it was subject to incorporation into the nanofibers.

Electrospinning of PVA nanofibers and gold nanocluster incorporated PVA nanofibers

The precursor PVA solution used for electrospinning was prepared by dissolving the PVA (7.5 Wt%) granules in deionised water at 80°C by gentle magnetic stirring for 6 hours. After the solution was brought to room temperature, various concentrations of gold cluster solution were added to the PVA solution. The processing parameters including viscosity (7.5 wt%), flow rate (0.5), applied voltage (10 kV) and distance between the electrodes (10cm) were subjected to optimization and further processed, bringing forth defect free PVA nanofibers and AuNC*NFs. The electrospinning process was carried out at room temperature in a closed plexiglass box. It is impulsive that the protracting collection time of 2-4 hours has retrieved self standing flexible fibrous membrane.

Cross-linking of Electrospun PVA and AuNC*NF mat

The cross-linking of PVA and AuNC*NF was carried out with glutaraldehyde (GA) vapour. Correspondingly, the GA solution was mixed with HCl (32 % w/v, as catalyst) in the volume ratio of 3:1 (GA: HCl). The resultant solution was spread out into a petri dish and placed at the bottom of the desiccator (20 cm (diameter) and 20 cm (height)). Then, PVA-NFM and AuNC*NFM were positioned into the sealed desiccator by using a metal wire without physical contact and exposed into a GA vapour atmosphere for 24 h. Consecutively, they were taken out of the desiccators and kept in a vacuum oven to remove the unreacted vapour molecules adsorbed by the samples.

Contact Mode Visual Detection of Hg^{2+}

As the next step in the process, the flexible nanofibrous membrane was cut uniformly into small pieces of size 2X3cm and then dipped in different concentrations of Hg^{2+} separately for 10 minutes. Subsequent to the solvent evaporation, the membrane was illuminated with UV light to study and confirm the colour changes. All the procedures were repeated and analyzed in order to ensure consistency in analysing the membrane. Similarly, the same procedure was continued and proceeded for different metal ions in water (Pb^{2+}, Cu^{2+}, Zn^{2+} etc) as well. For CLSM, the nanofibers were coated on separate glass slides and dipped in the Hg^{2+} solution for 2 minutes. After drying the solvent, images were taken at a magnification of 20X.

Instrumentation

Using scanning electron microscopy (SEM), the morphology and diameter of the nanofibers were measured (Quanta 200 FEG). The presence of elements in the AuNC*NF were analyzed by the application of Tecnai G2 F30-Transmission electron microscopy (TEM). Fluorescence emission spectrum was measured by the usage of time resolved fluorescence spectrophotometer (FL-1057 TCSPC). Confocal laser scanning microscopy (CLSM) images were recorded using Zeiss LSM 510, wherein excitation sources were fixed at

488 nm for all experiments and the images were captured at 20x magnification.

Result and Discussion

The design of the sensor strip is optimized on the basis of four decisive criteria here: (1) fine homogeneity of AuNC in the nanofibers (2) stability against time and temperature (3) insoluble nature of water (3) specific response to Hg^{2+} and (4) significant visual colorimetric detection. Collectively, the effort produced optimistic results. The SEM images of randomly oriented electrospun PVA nanofibers and AuNC*NFs, shows defect-free morphology with a relatively uniform diameter of 180 ± 40 nm, as depicted in the Fig. 1a and 1b.

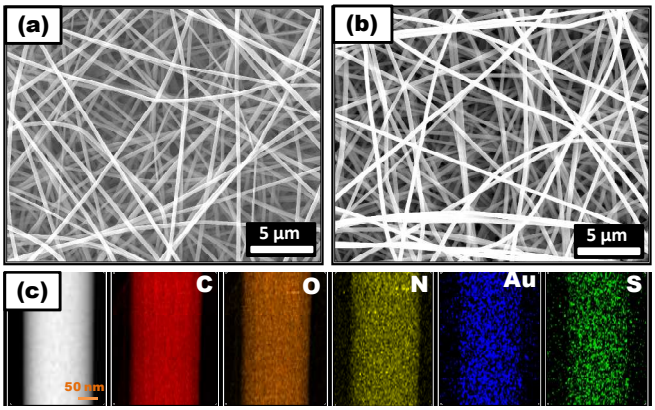

Fig. 1: SEM image of the PVA nanofibers (a) and gold nanocluster (4 wt%) embedded PVA nanofibers (NF) (b). (c) HAADF-STEM image and (High-angle annular dark- field scanning transmission-electron microscopy) mapping of the elements C, O, N, S and Au presents in the AuNC*NF.

Also, minute observation reveals the fact that the surface is rough compared to a bare PVA nanofibers, highlighting the partial exposure of the gold nanoclusters on the surface. Additionally, scanning transmission electron microscopy (STEM) elemental mapping of the AuNC embedded single PVA nanofiber results confirms that the spatial distribution of AuNC along the nanofiber is uniform as illustrated in Fig. 1c. This persistent allocation and configuration significantly enhances the purity and homogeneity of the color, which is of paramount repercussion for the colorimetric sensing properties. Furthermore, on exposure to UV light, the AuNC*NFM (366nm) emits a bright red fluorescence which is the characteristics emission of gold nanocluster, as shown in Fig. 2a-b. Confirming with the results, this approach marks a important in the field of retaining the original fluorescence efficiency of AuNC (see Fig. S1, ESI) in the PVA nanofibrous matrix, which is further established with the CLSM image (Fig. 2c-d). The observed fluorescence is uniform throughout the nanofibers, suggesting that the homogeneous distribution of gold nanocluster in the nanofibers. The uniformity and homogeneity of the nanofibers are mostly distorted by the varied concentration of the gold nanoclusters that are to be loaded. Initially, the effect of concentration of the AuNC in the polymer solution on the morphology of the electrospun nanofibers has been characterized using SEM as shown in Fig. S2, ESI. However, no discrete dissimilarity is seen with regard to the diameter as well the structure of the nanofibers. Moreover, variations in the proportional quantity of AuNC in the composite nanofibers has shown minute color discrepancies

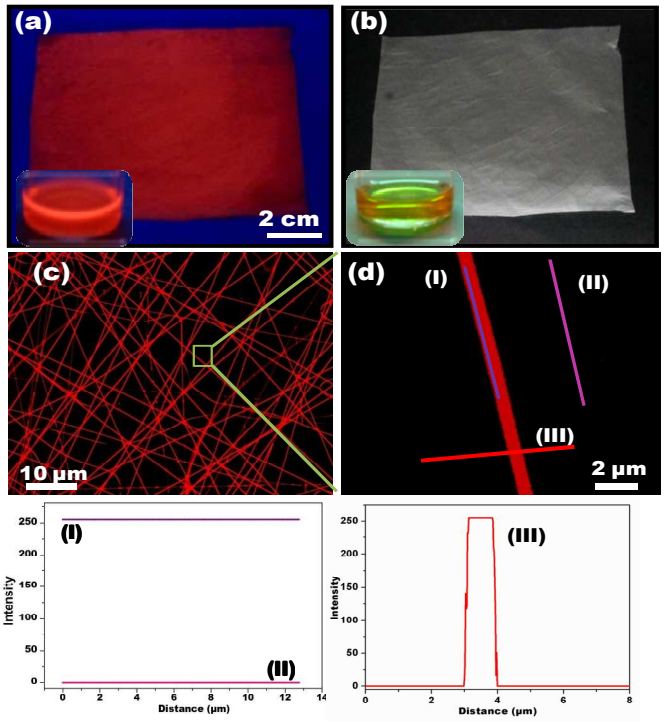

Fig. 2: Photographs of the AuNC*NFM under (a) UV light (λ_{ext} - 366 nm) and (b) white light. Inset shows the photograph of AuNC solution taken under the same condition (c) CLSM image of the AuNC*NFs excited at 488 nm (d) Isolated single AuNC*NF and their intensity data collected from their surface. The intensity reached maximum (I) on their NF surface and it is zero (II) where there is no NF. Further, measurement was carried out across the NFs (III).

ranging from a light red to a dark red color with respect to their increased concentrations (see Fig. 3a-e). Thus, the structural features and functional properties of the nanofibrous membranes can be effectively adjusted by tailoring the concentration of their AuNC constituents.

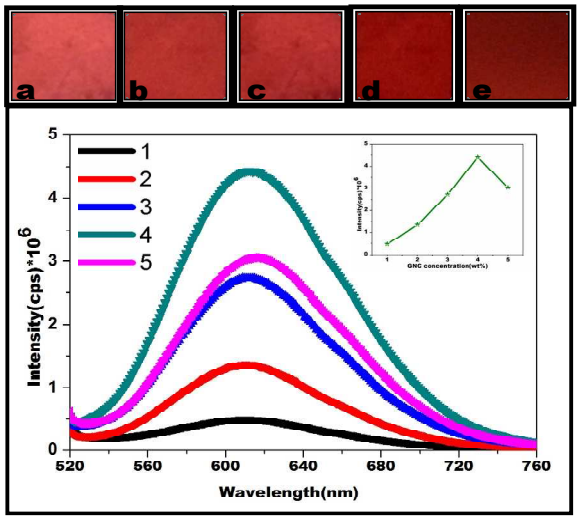

Fig. 3: Fluorescence spectra of AuNC*NFM with different concentrations of gold nanocluster (1-1 wt%, 2-2 wt%, 3-3 wt%, 4-4 wt% and 5-5 wt %) and their photographs taken under UV light (a-e)

Fig. 3 depicts the fluorescence spectra of AuNC*NFM with different concentrations of AuNC. As noticed in the spectra, the intensity of the emission is incremented to about 4 wt% of AuNC, followed by a gradual decrement with a shift towards the longer wavelength accompanied by the broadening of the peak.

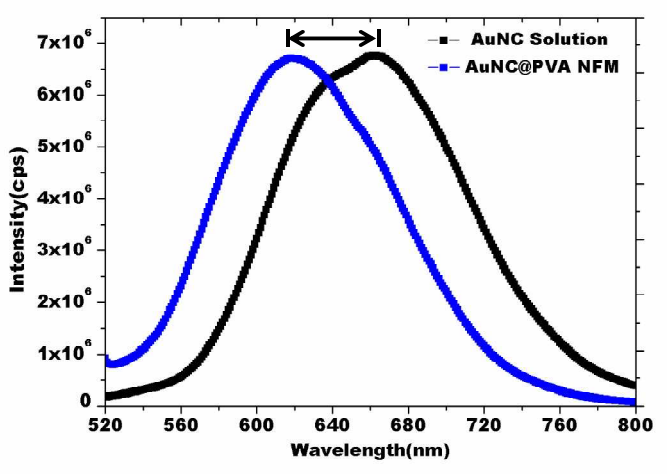

Fig 4: Compared emission spectra of AuNC solution and AuNC *NFM (λext-500 nm).

Analyzing the observations, this could be due to the increase in the concentration of AuNC, ultimately leading to a decrease in the inter particle distance in the nanofibrous film. Subsequently, this also shows a superlative result for the coupling effect between the nanoparticles, leading aggregation at higher concentrations.[34-36] However, the enlarged surface area, known for its rapid evaporation rate, proves to diminish the aggregation, because of which immediate solidification retards the further growth of the clusters inside the matrix.[37-40]

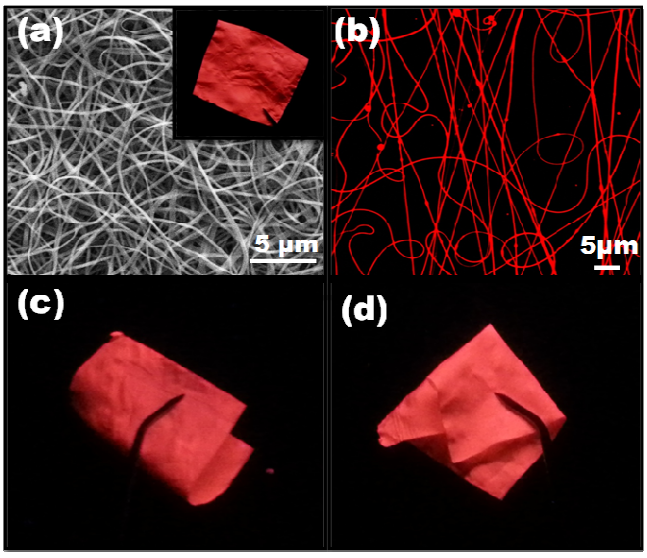

Fig. 5: (a) SEM image of the cross linked AuNC*NFM. Inset shows their photograph taken under UV light. (b) CLSM image of the AuNC*NFs (c & d) Flexibility nature of the nanofibrous membrane.

Secondly, the AuNC have a tendency to be sensitive to factors including nature of the ligands, size, environment and temperature.[41-42] The compared photoluminescence spectra of AuNC solution and AuNC*NFM is shown in Fig. 4, ESI. Understanding from the spectra, it is evident that the deconvoluted spectra marks a confirmation on the presence of two bands, originating from the stable Au-core (Band I) and Au-S (Band II), as illustrated in Fig. S3, ESI.[43] There is also a remarkable phenomenon observed at this juncture that the fluorescence emission of AuNC*NFM shows an elegant blue shift with a declined bandwidth, when compared to the results shown in the solution state. With further study into the results, it is noticed that these happenings might be arises from the two reason: (1) strong confinement and well organized nature of the cluster assembly in the nanofibrous matrix (2) Polarity of the local environment of the gold nanoclusters i.e the local dielectric environment of AuNCs in the nanofibers have less polarity than that of Au NCs dispersed in solution.[44-45]

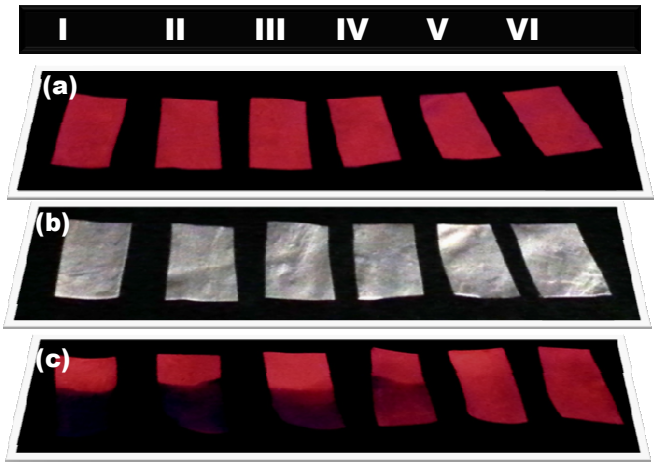

Fig. 6: Visual colorimetric detection of Hg2+ by contact mode approach (a-b) Photograph of the AuNC*NFM strip before Hg^{2+} treatment under viewed UV and white light (c) Fluorescence quenching of AuNC*NFM strips by different concentration of Hg^{2+} when viewed under UV light (I-1 ppm, II-100 ppb, III-50 ppb, IV-20ppb, V-10ppb, VI-1 ppb). Half a piece of the membrane strip is dipped in the Hg^{2+} solution and other half is maintained as a reference to clear visualization of color change.

We subsequently evaluated the fluorescence stabilities of AuNC*NF since the AuNC emissions in solution state decreased with time when exposed to typical atmosphere at room temperature. This detriments the development of practical application of these sensors. In the present case, the nanofibrous membrane is subjected at room temperature for a prolonged period of time; say 1 to 6 months and then CLSM images have been recorded (see Fig S4, ESI). The observed results confirm that there is no considerable decrease in the emission intensity and the AuNC*NFM continues to maintain the red fluorescence under UV light. Suggestive measures state that the wrapping of polymer chains around the fluorescent nanoclusters provides the protective environment, thereby improving the AuNC stability. Thus the electrospun nanofibers not only enhances the stability of the system, but also retains its characteristic emission features stressing on their extended storability and usability.

To elucidate the thermal stability of AuNC*NFM, the membrane was treated at different temperature ranges from 50ºC to 175ºC. Fig S5, ESI shows the luminescence profiles with the photographs of the AuNC*NFM treated at different temperatures. As expected, the intensity is shown to be increased at 50ºC resulting due to the removal of water molecules adsorbed on the surface. The fluorescence feature of AuNC*NFM is well maintained at around 100ºC which implies the fact that the membranes are more durable against heat. This emerges to be a satisfying attribute for outdoor sensor applications. In correspondence to the process, subsequent thermal annealing beyond 100ºC drastically has decreased the emission intensity of the sensor.

The undetermined blue-shifts have resulted from the reduced stability of the surface in nanoclusters which are known to be caused by the degradation of BSA. We have thus obtained a distinct fluorescence emission change and the subsequent nanofiber structure has finally not been changed as illustrated in Fig. S6, ESI. The obtained nanofibrous mat was found to be instantaneously soluble in water. Hence, the AuNC*NFM further gets cross linked with glutaraldehyde vapour.[46-48] As observed in Fig. 5, the morphology (a) and the fluorescence nature (b) of the nanofibers remain unchanged after cross linking. It suggested that the spatial distribution of the AuNC is kept unchanged which was further confirmed by HAAD-STEM mapping (Fig.S7). Its stability has been tested by immersing the membrane in water for 24 hours and their unaffected morphology has proved their durability (see Fig. S8, ESI). The flexible nature of the cross linked NFM doesn't alter even though the membrane becomes trivially hard compared with as-spun NFM, which is clearly observed in Fig. 5c and d.

efficiently than the interfacially segregated AuNC in the solution casting film. Besides, an electrospun nanofiber enables the expedient diffusion of analyte molecules into the nanofibrous matrix accelerating the sensitive response of Hg^{2+} mercury sensing.[49-50] The sensing performance of AuNC*NFM towards the mercury ions in the aqueous solution have been tested in diverse approaches of (a) fluorescence spectra (b) Visual colorimetric response through the contact mode and CLSM based analysis. The equilibrium fluorescence quenching has been reached within 10 minutes which might results from the rapid interaction between the analytes and gold nanocluster (See Fig.S9). Therefore, the AuNC*NFM strip is immersed in the Hg^{2+} solution for 10 minutes and then taken out from the solution for further studies. The variation in the emission features of AuNC*NFM have been supervised upon exposure to different concentrations of Hg^{2+}, by fluorescence spectra as depicted in Fig. S10, ESI. Apparently, the fluorescence intensity is shown to decrease with increasing concentrations of Hg^{2+} due to the strong metallophilic bond established between Hg^{2+} and Au^{+}.[51-53] Noticeably, the detection limit is concluded to give a valuable limit of 0.1 ppb according to the U.S. EPA which has defined a maximum contamination level of mercury in drinking water as 2 ppb. The morphology of the AuNC*NFM is not affected after addition of Hg^{2+} is shown in Fig. S11, ESI.

Further, an intention to analyze the visual colorimetric response of the sensor strips toward various concentrations of Hg^{2+} has been intended. Firstly, the membrane strip is immersed in water in the absence of Hg^{2+}. This resulted in insignificant changes in their fluorescence behavior when viewed in naked eye. For apparent visualization, half a piece of

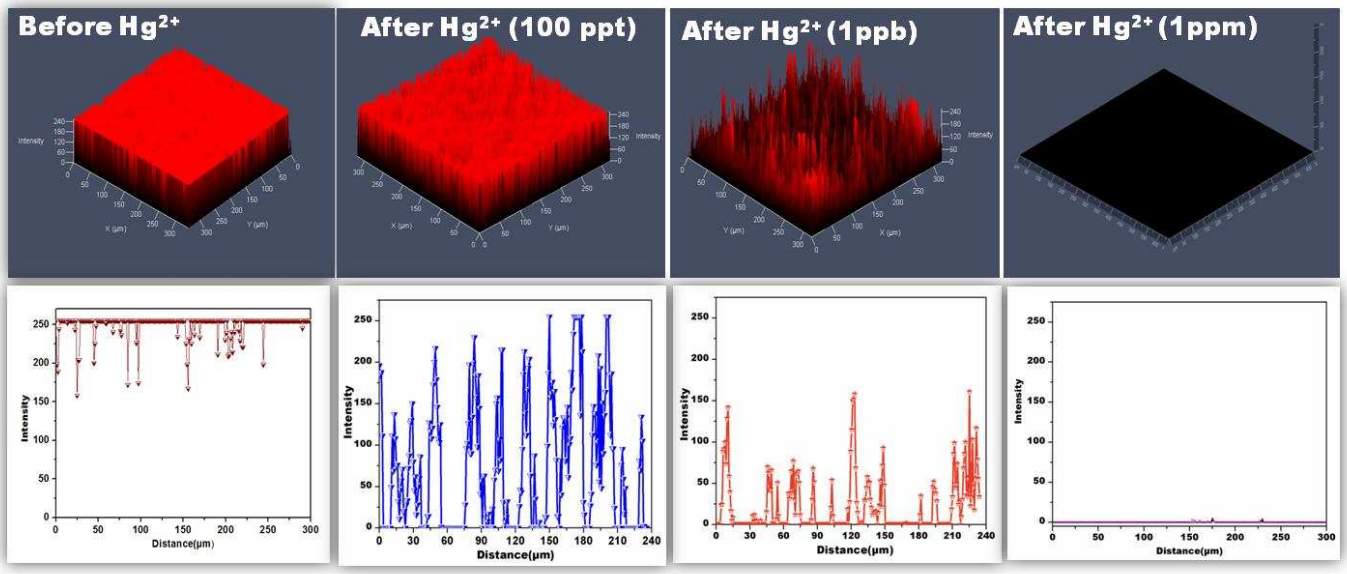

Fig. 7: CLSM images of the AuNC*NFs before and after treatment of Hg^{2+} and their intensity data collected across the nanofibrous membrane surface (λ_{ext} = 488 nm, 20x magnification)

As a known parameter in sensor performance, the metal ion selectivity and binding kinetics are strongly dependent on the morphology of the sensor system, acting as a leading force towards the phenomenon of fluorescence quenching. Also, partially dispersed gold nanoclusters in the electrospun nanofibers are expected to quench the fluorescence more

the membrane strip is dipped into the mercury solution and the other half is maintained as a reference clearly depicted in Figure 6. Attractively, the sensor displayed distinguishable color changes from red to dark blue upon the increase of Hg^{2+} concentration, detectable with the naked eye upto 50 ppb. However, even though there has been a decrease in the red

color upon decline in concentrations, changes have not been visible below the described concentration.

The mechanism for changes of color upon exposure to Hg^{2+} can be understood as follows. The higher surface area in the nanofibers facilitate the more adsorption Hg^{2+} ions on their surface resulted in rapid desorption of capping molecules from the AuNC surface which leads to changes of color from red to blue. The observed changes in color couldn't be retained even after prolonged time indicating that there could be adsorption of Hg^{2+} on the surface of AuNC. Additionally, the sensor strips fabricated from different batches exhibited identical sensing responses which implies that the consistent of the performance.

Typically, the incubation time is periodically long (~10 to 30 minutes) to observe the visual response of the sensor. Exploring more into the function of the detection system for Hg^{2+}, the sensing performance of mercury is displayed by the method of CLSM, as depicted in Fig. 7. Conspicuously, the visual detection limit is extended up to 1 ppb and differences in the fluorescence intensity are monitored within a time frame of 2 minutes. Deliberately, the competing chemical interferences of the toxic metal ions in water poses a problem with the conventional detection approach for selective determination of mercury. Subsequently, selectivity has been investigated by testing the response of the sensor towards Pb^{2+}, Cd^{2+}, Mg^{2+}, Cu^{2+}, $Zn^{2+}$and Co^{2+} at higher concentrations, say 10 ppm and the corresponding visual fluorescence response is illustrated in Fig. 8.

It is interesting to note that except for Hg^{2+}, no obvious deviations has been observed where in contrast it has been found that the Cu^{2+} ions revealed a slight decrease in their fluorescence intensity. However, as the concentration goes down, there hasn't been any more quenching for Cu^{2+} ions, and additionally luminescence was completely quenched for Hg^{2+}.

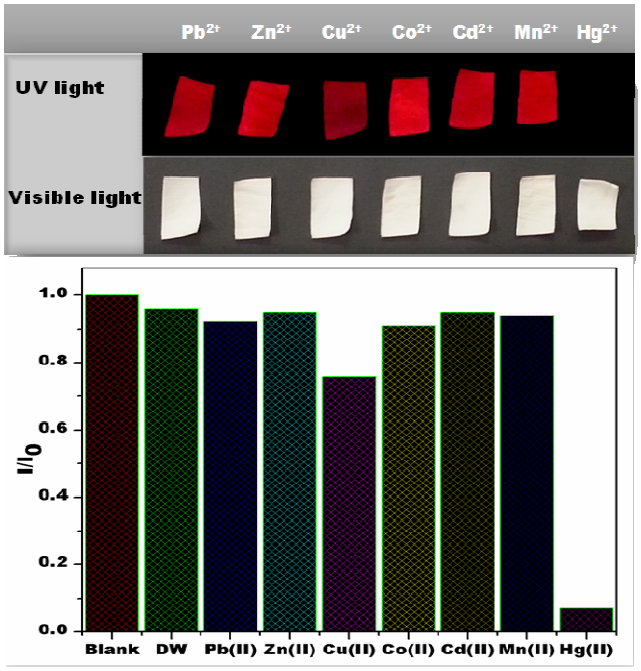

Fig. 8: Sensing performance of AuNC*NFM upon exposure to different metal ions in water. The concentration of all metal ions were fixed at 10 ppm. Photographs were taken under UV and white light.

Besides, no color change has been viewed for the other ions except Hg^{2+}, with its original color being retained. This exclusive and unique color change of Hg^{2+} treated membrane strip substantiates the fact that the selective detection could also be visualized with the naked eye.

Conclusions

To conclude, highly fluorescent and flexible AuNC*NFM have been produced by a proficient method of electrospinning, exhibiting solid stability and steadiness over extended periods of time in an applicable environment constituting of temperatures up to 100ºC. A successful and profitable procedure has been taken up for the preparation of the water stable membrane by cross linking the resultant membrane with glutaraldehyde vapour. Evidently, this has stood up as the first ever example showcasing the incorporation of the fluorescent gold clusters in the electrospun nanofibers for the efficient detection of Hg^{2+} in aqueous solutions. The resultant color change coupled with the selective coordination of Hg2+ has successfully demonstrated the trouble-free "naked eye" colorimetric sensing. The stunning features of high stability, sensitivity and selectivity have given all the limelight necessary for the sensor, implicating its practical applications in the environmental monitoring of toxic mercury. However, more intense research needs to be encouraged on the betterment of the sensitivity of the system towards visual colorimetric detection. Inspiringly, studies have been initiated to explore more on the discussed topic.

Acknowledgements

A.S. thanks the Scientific & Technological Research Council of Turkey (TUBITAK) (TUBITAK-BIDEB 2216, Research Fellowship Programme for Foreign Citizens) for postdoctoral fellowship. A.C. acknowledges TUBITAK-BIDEB for the national Ph.D. study scholarship. T.U acknowledges partial support of EU FP7- Marie Curie-IRG for funding NANOWEB (PIRG06-GA-2009-256428) and The Turkish Academy of Sciences - Outstanding Young Scientists Award Program (TUBA-GEBIP). Authors thank M. Guler for TEM-STEM analysis.

Notes and references

[a]UNAM-National Nanotechnology Research Centre, Bilkent University, Ankara, 06800, Turkey.
[b]Institute of Materials Science & Nanotechnology, Bilkent University, Ankara, 06800, Turkey.
AS:senthamizhan@unam.bilkent.edu.tr;
TU: uyar@unam.bilkent.edu.tr

Electronic Supplementary Information (ESI) available: [details of any supplementary information available should be included here]. See DOI: 10.1039/b000000x/

1 EPA, U.S., EPA, U.S., Drinking Water Contaminants, 〈http://water.epa.gov/drink/contaminants/index.cfm#List〉 (Accessed on 31 12 11).
2. EPA (US Environmental Protection Agency) established the mercury(II) limit on 2 ppb, 2006, EPA-HQ-OPPT-2005-0013
3. Z. Zhu, Y. Su, J. Li, D. Li, J. Zhang, S. Song, Y. Zhao, G. Li, and C. Fan, *Anal. Chem*. 2009, **81**, 7660.
4. W. R. Hatch and W. L. Ott, *Anal. Chem*., 1968, **40**, 2085.
5. J. H. An, S. J. Park, O. S. Kwon, J. Bae, and J. Jang, *ACS Nano*, 2013, 7, 1056.

6. T. Balaji, A. Sherif, E. Safty, H. Matsunaga, T. Hanaoka, and F. Mizukami, *Angew. Chem. Int. Ed*. 2006, ***45***, 7202.
7. Q. Wei, R. Nagi, K. Sadeghi, S. Feng, E. Yan, S. J. Ki, R. Caire, D. Tseng, and A. Ozcan, *ACS Nano*, 2014, **8**, 1121.
8. W. Ren, C. Zhu and E. Wang, *Nanoscale*, 2012, **4**, 5902.
9. G.L. Wang, J.J. Xu and H.Y. Chen, *Nanoscale*, 2010, **2**, 1112.
10. H. N. Kim, W. X. Ren, J. S. Kim and J. Yoon, *Chem. Soc. Rev*., 2012, **41**, 3210.
11. P. Wu, T. Zhao, Shanling Wang and Xiandeng Hou., *Nanoscale*, 2014, **6**, 43.
12. J. Zhang and S.H. Yu, *Nanoscale*, 2014, DOI: 10.1039/c3nr05896d.
13. G. S. Anand, A. I. Gopalan, S.-W. Kang and K.-P. Lee, *J. Anal. At. Spectrom*., 2013, **28**, 488.
14. J. Liu, X. Ren, X. Meng, Z. Fang and F. Tang, *Nanoscale*, 2013, **5**, 10022.
15. D. Lu, C. Zhang, L. Fan, H. Wu, S. Shuang and C. Dong, *Anal. Methods*, 2013, **5**, 5522.
16. X. Yuan, T. J. Yeow, Q. Zhang, J. Y. Lee and J. Xie, *Nanoscale*, 2012, **4**, 1968.
17. X. Yuan, Z. Luo, Y. Yu, Q. Yao, and J. Xie, *Chem. Asian J*., 2013, **8**, 858.
18. S. Chen, D. Liu, Z. Wang, X. Sun, D. Cui and X. Chen, *Nanoscale*, 2013, **5**, 6731.
19. Y. Si, X. Wang, Y. Li, K. Chen, J. Wang, J. Yu, H. Wang and B. Ding, *J. Mater. Chem. A*, 2014, **2**, 645.
20. Y. Zhang, L. Gao, L. Wen, L. Heng and Y. Song, *Phys. Chem. Chem. Phys*., 2013, **15**, 11943.
21. D. Wang, K. Zhou, M. Sun, Z. Fang, X. Liu and X. Sun, *Anal. Methods*, 2013, **5**, 6576.
22. N. Vasimalai and S. Abraham John, *J. Mater. Chem. A*, 2013, **1**, 4475.
23. Z. Lin, F. Luo, T. Dong, L. Zheng, Y. Wang, Y. Chi and G. Chen, *Analyst*, 2012, ***137***, 2394.
24. A. Jaiswal, S. S. Ghsoh, and A. Chattopadhyay, *Langmuir*, 2012, **28**, 15687.
25. H. Ahn, S. Y. Kim, O. Kim, I. Choi, C.-H. Lee, J. H. Shim, and M. J. Park., *ACS Nano*, 2013, **7**, 6162.
26. W. Xiao, Y. Luo, X. Zhang and J. Huang, *RSC Adv*., 2013, *3*, 5318.
27. X. Zhang and J. Huang, *Chem. Commun*., 2010, **46**, 6042.
28. L. Su, T. Shu, Z. Wang, J. Cheng, F. Xue, C. Li , X. Zhang, *Biosens. Bioelectron*., 2013, **44**, 16.
29. N. Liu, L. Li, G. Cao and R. Lee, *J. Mater. Chem*., 2010, **20**, 9029.
30. L. Q. Xu, K.-G. Neoh, E.-T. Kang and G. D. Fu, *J. Mater. Chem. A*, 2013, **1**, 2526.
31. J. H. Wendorff, S. Agarwal, A. Greiner, Electrospinning: Materials, Processing, and Applications; Wiley-VCH Verlag GmbH & Co. KGaA, 2012.
32. S. Ramakrishna, K. Fujihara, W. Teo, T. Lim, Z. Ma, World Scientific Publishing Company: Singapore, 2005.
33. J. Xie, Y. Zheng, and J. Y. Ying, *JACS*, 2009, **131**, 888.
34. A. C. Balazs, T. Emrick, T. P. Russell, *Science*, 2006, *314*, 1107.
35. X. Yu, D. Y. Lei, F. Amin, R. Hartmann, G. P. Acunac, A. Guerrero-Martínez, S. A. Maier, P. Tinnefeld, S. Carregal-Romero, W. J. Parak, *Nano Today*,2013, **8**, 480.
36. R. Elghanian, J. J. Storhoff, R. C. Mucic, R. L. Letsinger, C. A. Mirkin, *Science*, 1997, **277**, 1078.
37. Y. Bao , H. Fong and C. Jiang, *J. Phys. Chem. C*, 2013, **117**, 21490.
38. P. Wang, L. Zhang, Y. Xia, L. Tong, X. Xu, Y. Ying, *Nano Lett*., 2012, **12**, 3145.
39. H. Zhu, M. Du, M. Zou, C. Xu, N. Lia, and Y. Fu, *J. Mater. Chem*, 2012, **22**, 930.
40. C. H. Lee, L. Tian, A. Abbas, R. Kattumenu and S. Singamaneni, *Nanotechnology*, 2011, **22**, 27531.
41. Z. Wu and R. Jin, *Nano Lett*. 2010, **10**, 2568.
42. S. Goel, K. A. Velizhanin, A.Piryatinski, S.A. Ivanov, S. Tretiak, *J. Phys. Chem. C*, 2012, **116**, 3242.
43. Xi. Wen, P. Yu, Y.R. Toh, and J. Tang, *J. Phys. Chem. C*, 2012, **116**, 11830.
44. K. E. Roskov, K. A. Kozek, W.-C. Wu, R. K. Chhetri, A. L. Oldenburg, R. J. Spontak, and J.B. Tracy, *Langmuir*, 2011, **27**, 13965.
45. C.-L. Zhang, K.P. Lv, H.-P. Cong, S.-H. Yu, *Small*, 2012, **8**, 648.
46. A. G. Destaye, C.K. Lin and C.-K. Lee, *ACS Appl. Mater. Interfaces* 2013, **5**, 4745.
47. J. Wang, H.-B. Yao, D. He, C.-L. Zhang, S.-H. Yu, *ACS Appl. Mater. Interfaces*, 2012, **4**, 1963.
48. C. Tang, C. D. Saquing, J. R. Harding, S. A. Khan, *Macromolecules*, 2010, **43**, 630.
49. Y. Si, X.Wang, Y. Li, K. Chen, J. Wang, J. Yu, H.Wang and B. Ding, *J. Mater. Chem*. A, 2014, **2**, 645.
50. X. Wang, Y. Si, X. Mao, Y. Li, J. Yu, H. Wang and B. Ding, **Analyst**, 2013, **138**, 5129.
51. Y. Si, X. Wang, Y. Li, K. Chen, J.Wang, J. Yu, H.Wang and B. Ding, *J. Mater. Chem. A*, 2014, **2**, 645.
52. J. Xie, Y. Zheng and J. Y. Ying, *Chem. Commun*., 2010, **46**, 961.
53. J.-S. Lee, M. S. Han, and C. A. Mirkin, *Angew. Chem. Int. Ed*., 2007, **46**, 4093.

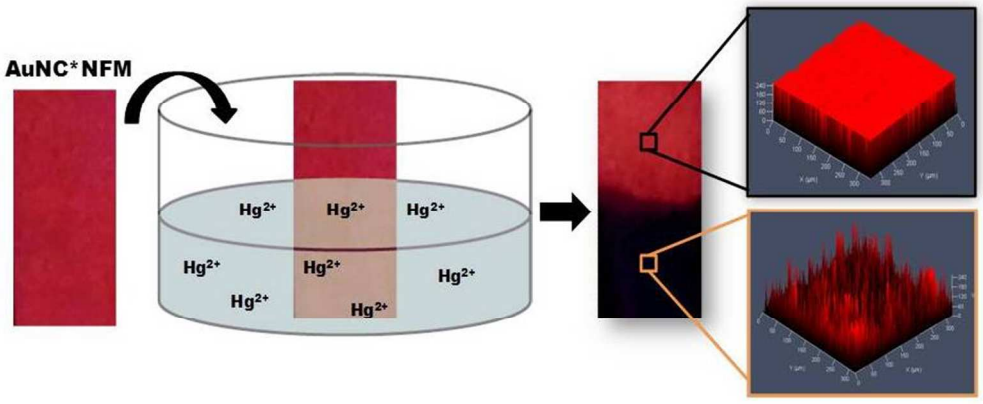

251x107mm (96 x 96 DPI)